ACS NANO
Cite This: ACS Nano 2018, 12, 12464–12471
www.acsnano.org

ARTICLE

Aqueous Stable Ti_3C_2 MXene Membrane with Fast and Photoswitchable Nanofluidic Transport

Junchao Lao,[†] Ruijing Lv,[†] Jun Gao,*[,‡] Aoxuan Wang,[†] Jinsong Wu,[§] and Jiayan Luo*[,†,⊥]

[†]Key Laboratory for Green Chemical Technology of Ministry of Education, State Key Laboratory of Chemical Engineering, School of Chemical Engineering and Technology, Tianjin University & Collaborative Innovation Center of Chemical Science and Engineering (Tianjin), Tianjin 300072, China

[‡]Physics of Complex Fluids, University of Twente, Enschede 7500AE, The Netherlands

[§]State Key Laboratory of Advanced Technology for Materials Synthesis and Processing, Wuhan University of Technology, Wuhan 430070, China

[⊥]Key Laboratory for Advanced Energy Materials Chemistry (Ministry of Education), Nankai University, Tianjin 300071, China

Supporting Information

ABSTRACT: **High, stable, and modulatable ionic conductivity is important for many nanofluidic applications of layered two-dimensional (2D) membranes. In this study, we demonstrate a proton and ionic conductivity of the $Ti_3C_2T_x$ membrane that is orders of magnitude higher than that of bulk solution at low concentrations. Importantly, the membrane is highly stable in aqueous solution without any modification, due to the strong and attractive interlayer van der Waals interaction and weak electrostatic repulsive interaction. Furthermore, by exploiting the intrinsic photothermal property of MXene, we demonstrate that the ionic conductivity can be reversely, rapidly, and completely switched on or off with laser light. This study should prove MXene membrane as a suitable platform to study and utilize nanofluidic ion transport. It should also inspire future studies to manipulate the mass transport through 2D membranes using their inherent physicochemical properties.**

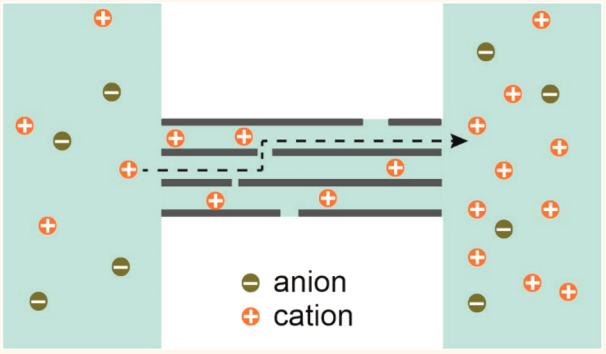

KEYWORDS: *MXene, nanofluidic, aqueous stability, photocontrolled, surface charge*

Two-dimensional (2D) nanosheets dispersed in solution naturally restack into a laminar structured membrane when dried.[1] The spacing between the stacked sheets forms massive interconnected nanochannels with highly uniform size, typically ranging from sub-nanometer to a few nanometers,[1−5] which is comparable to the size of hydrated ions. As a result, the ion transport through the membrane is largely dictated by the surface properties of the nanochannels, enabling a broad range of properties.[3,6−10] Previous study revealed that the ionic conductivity of the graphene oxide (GO) membrane is determined by the surface charge of the nanochannels at electrolyte concentration up to physiological conditions[8] and is orders of magnitude higher than that of bulk, which is termed surface-charge-governed transport.[11] Such a phenomenon has also been observed on 2D layered clay,[3] boron nitride,[10] and polymeric carbon nitride[12] membranes. The high ionic conductivity (or high ionic permeability) of 2D layered membranes is important for a broad range of nanofluidic applications,[2,13,14] such as molecular sieving,[6] water treatment,[7,15,16] energy conversion,[17,18] energy storage,[19−23] and battery separators.[24,25] The field of 2D nanofluidics is receiving growing interest[2,4,9] thanks to its high versatility, high scalability, precise and tunable channel size, and high flux.[2]

However, the GO membrane, as well as some other 2D layered membranes, including clay, has an inherent limitation: it disintegrates in an aqueous environment due to the strong electrostatic repulsion forces between nanosheets.[26] Cross-linking[15,26] or reduction[18] is generally needed to fabricate stable membrane. Yet, cross-linking brings complexity to the structure, and cross-linking cations could be exchanged by external ions.[27] Reduction, on the other hand, compromises the hydrophilicity of the GO membrane.[28] Therefore,

Received: September 2, 2018
Accepted: November 29, 2018
Published: November 29, 2018

DOI: 10.1021/acsnano.8b06708
ACS Nano 2018, 12, 12464−12471

searching for an inherently aqueous stable 2D layered membrane is crucial to expand nanofluidic applications. For example, a pioneering work demonstrated the excellent aqueous stability of MoS_2 membranes.[29] The key factors underpinning aqueous stability are stronger van der Waals attraction force, as demonstrated by Wang *et al.*, with a MoS_2 membrane[30] and weaker electrostatic repulsion force.

Furthermore, a smart nanofluidic system which allows real-time on-demand modulation of transport is of particular interest.[31] However, most conventional smart nanofluidic systems rely on chemical modification of responsive soft matters,[31] which not only complicates the fabrication process but also has relatively low modulation efficiency. Recently, smart graphene oxide separation membrane[32] has been realized by covalently binding temperature-responsive poly(*N*-isopropylacrylamide), which results in a gating ratio of around 7. An ideal smart membrane, however, should allow switching completely on and off with high efficiency. Recent studies have demonstrated that, by exploiting the electrical properties of graphene oxide or reduced graphene oxide, the mass transport can be switched between ultrafast to complete blocking,[33] and the ion diffusion can be modulated easily with low voltage.[34] These results suggest that controlling mass transport with 2D layered membranes could be easy by exploiting their intrinsic physical properties.

MXene,[35] a family of 2D materials with the form of $M_{n+1}X_nT_x$, where M represents an early transition metal, X represents carbon or nitrogen, n = 1, 2, or 3, T represents surface groups (−O, −OH, and/or −F), and x is the number of terminating groups. MXene has shown promising potential for energy storage[36−39] and water treatment.[40,41] However, its nanofluidic transport properties, which are crucial for its applications, remain rarely studied. Its aqueous stability, although indicated by several studies, remains poorly understood.[38,42] Some studies utilized MXene membranes in concentrated electrolyte solution, which are known to contaminate 2D membranes and screen the surface charge of 2D nanosheets,[26] thereby baffling the reflection of the membrane's inherent property, and lack practical relevance to applications in dilute electrolyte conditions. Validating the neat MXene membrane's stability and resolving its mechanism are therefore of great importance. In this work, we demonstrate that the MXene membrane is a nanofluidic platform exhibiting fast, stable, and modulatable ion transport properties. Its ionic conductivity is 1−2 orders of magnitude higher than that of bulk at low electrolyte concentrations. Moreover, we reveal that its high stability in water arises from the nearly 1 order of magnitude stronger van der Waals attraction force and 2 orders of magnitude weaker electrostatic repulsion force compared to that of GO. This will allow facile aqueous applications of the MXene membrane without the need for any modification. Furthermore, by making use of the photothermal effect of the MXene membrane, we demonstrate that the nanofluidic flow can be completely, quickly, and reversibly switched on and off with laser light.

DISCUSSION

Assembly of Nanofluidic Devices. A 2D titanium carbide is used in this study to demonstrate the nanofluidic properties of MXene. As illustrated in Figure 1a, bulk Ti_3AlC_2 (left scheme) was etched with hydrofluoric acid to remove the Al layer and then exfoliated into nanosheets with the help of dimethyl sulfoxide intercalation.[43] The dispersed nanosheets

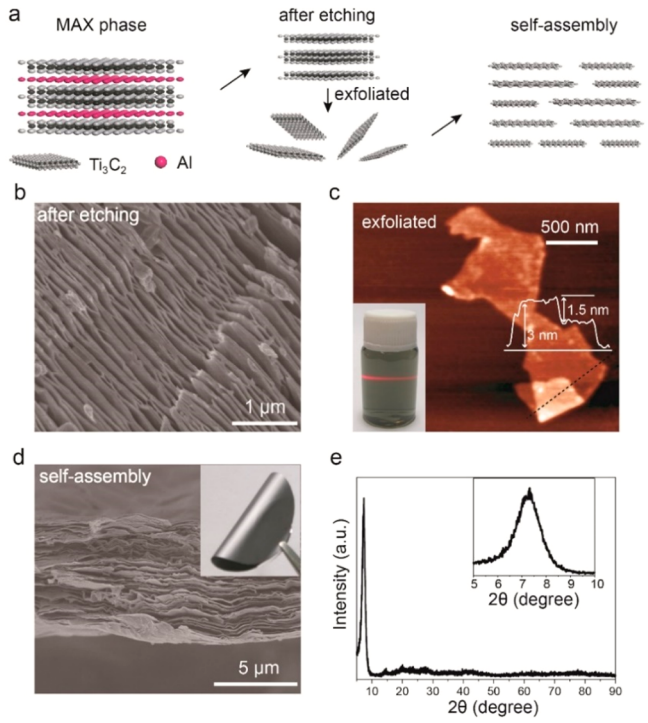

Figure 1. Fabrication and characterization of MXene membrane. (a) Schematic illustration of the fabrication process. Bulk Ti_3AlC_2 (left) was etched to remove the Al layer and exfoliated into nanosheets (middle), followed by self-assembling into a layered membrane (right) upon vacuum filtration. (b) SEM image of the etched bulk Ti_3AlC_2, showing its layered crystalline structure. (c) AFM image of an exfoliated nanosheet with a thickness of 1.5 nm and width of several hundreds of nanometers, typical for a single-layer MXene. Inset shows the Tyndall effect of the MXene solution, suggesting the colloidal feature. (d) Cross-sectional SEM image of the self-assembled MXene membrane, showing its ordered laminar structure. Inset is an optical image of the membrane. (e) XRD pattern of the dry membrane, showing a single strong peak at 7.3°, indicating a uniform layer spacing of 1.21 nm. Inset: magnified view of the peak.

(middle scheme) self-assembled into a nanofluidic membrane (right scheme) upon vacuum filtration on a polypropylene filter membrane (Celgard 2400), which avoids unintentional cross-linking. Such a fabrication method has been commonly used in previous works, allowing the studied nanofluidic properties to have broader meaning. After etching and before exfoliation, the sample has a layered crystal structure, as shown by the scanning electron microscopy (SEM) image (Figure 1b). After exfoliation, the MXene nanosheets are well dispersed in water, as suggested by the Tyndall effect (optical image in the inset of Figure 1c). The nanosheets are typically several hundreds of nanometers to micrometers in lateral size and 1.5 nm in thickness, as shown by the atomic force microscopy (AFM) image (Figure 1c), which is in accordance with previous studies.[44] Transmission electron microscopy (TEM) confirmed the high crystallinity of the nanosheets (Figure S1). X-ray photoelectron spectroscopy (XPS) identified hydrogen and fluorine on MXene (Figure S2), indicating the existence of hydroxide and fluoride surface groups. These groups impart the nanosheets with negative charge in water and the membrane with cation selectivity, as also suggested by the negative ζ-potential of the MXene colloid (Figure S3). After self-assembly, the MXene membrane

DOI: 10.1021/acsnano.8b06708
ACS Nano 2018, 12, 12464−12471

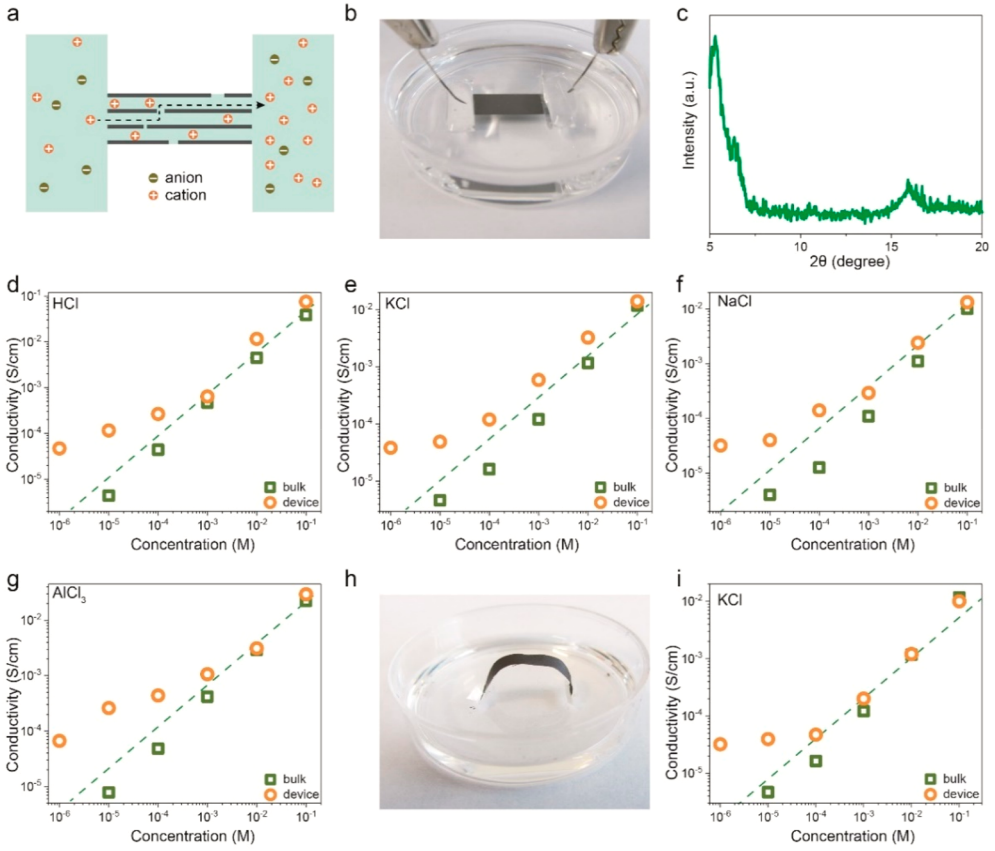

Figure 2. Nanofluidic transport property of the MXene membrane. (a) Schematic illustration and (b) optical image of the nanofluidic device. Due to the negative charge of the MXene nanosheets, cations are the major charge carriers, which transport through the interconnected nanofluidic channels. (c) XRD pattern of the hydrated membrane. The strong peak at 5.3° suggests an enlarged layer spacing of 1.67 nm. Representative ionic conductivities of the membrane as a function of concentration for various electrolytes: HCl (d), KCl (e), NaCl (f), and $AlCl_3$ (g). The conductivities are much higher than those of bulk at low concentrations, which is a typical behavior of surface-charge-governed transport. (h,i) MXene membrane for flexible nanofluidic device. (h) Optical image of the device. (i) Typical ionic conductivities for KCl, suggesting that the surface-governed transport is well kept. Dashed lines are a guide for the eye.

(optical image in the inset of Figure 1d) recovers the highly ordered layered structure (SEM image in Figure 1d). Meanwhile, its layer spacings form massive interconnected nanofluidic channels (right scheme of Figure 1a). This porous network allows the transport of ions, even though a single MXene sheet is nonporous. X-ray diffraction (XRD) pattern shows a strong and single peak at 7.3°, suggesting the highly uniform lamellar structure of the membrane with a layer spacing of 1.21 nm (Figure 1e). The channel size (free layer spacing) is therefore estimated to be around ∼0.2 nm, after subtracting ∼1 nm thickness of a clean MXene nanosheet. This size is even smaller than a water molecule (∼0.3 nm) and therefore does not allow ionic transport. Then the obtained MXene membrane was cut into a rectangular shape and embedded in a polydimethylsiloxane (PDMS) matrix.[8] After that, two electrolyte reservoirs were carved out at the two ends of the MXene membrane (Figure 2a,b). Before the conductivity measurement, the membrane was immersed in deionized (DI) water for 24 h to allow full hydration (Figure S4). After hydration, the interlayer spacing increased to 1.67 nm, as suggested by the strong peak at 5.3° on the XRD pattern (Figure 2c), suggesting a channel size of ∼0.67 nm, larger than that of water molecules, and enough to transport many hydrated ions.

Ionic Conductivity of MXene Membranes. Ionic currents through the MXene membrane were measured under sweeping voltages to derive its conductance in various electrolyte solutions including HCl, KCl, NaCl, and $AlCl_3$ of various concentrations. Before testing each concentration of each electrolyte, the membrane was immersed in testing electrolyte for 24 h to ensure a stable current (Figure S4). When the voltage is applied, ions will be driven through the interconnected nanochannels (schematic illustration in Figure 2a). Control experiments were carried out to confirm that the measured ionic current is mainly due to the transport of ions (see Supporting Information and Figure S4 for details). Figure 2d shows the typical conductivity results for protons (HCl, orange circles). As a comparison, the conductivity of the bulk HCl solution was also measured and presented (green squares). Obviously, the bulk conductivity is almost linearly proportional to the HCl concentration (dashed line is a guide for the eye). The conductivity of the membrane, however, exhibits a distinct behavior. At high concentrations ($\geq 10^{-3}$ M), the membrane conductivity is almost the same as that with the bulk. At lower concentrations, the conductivity deviates from the bulk behavior and is about 1−2 orders of magnitude higher than that of the bulk. This is a typical behavior of surface-charge-governed transport.[3,8,11] In water, the MXene nanosheet carries a negative charge due to the disassociation of

DOI: 10.1021/acsnano.8b06708
ACS Nano 2018, 12, 12464−12471

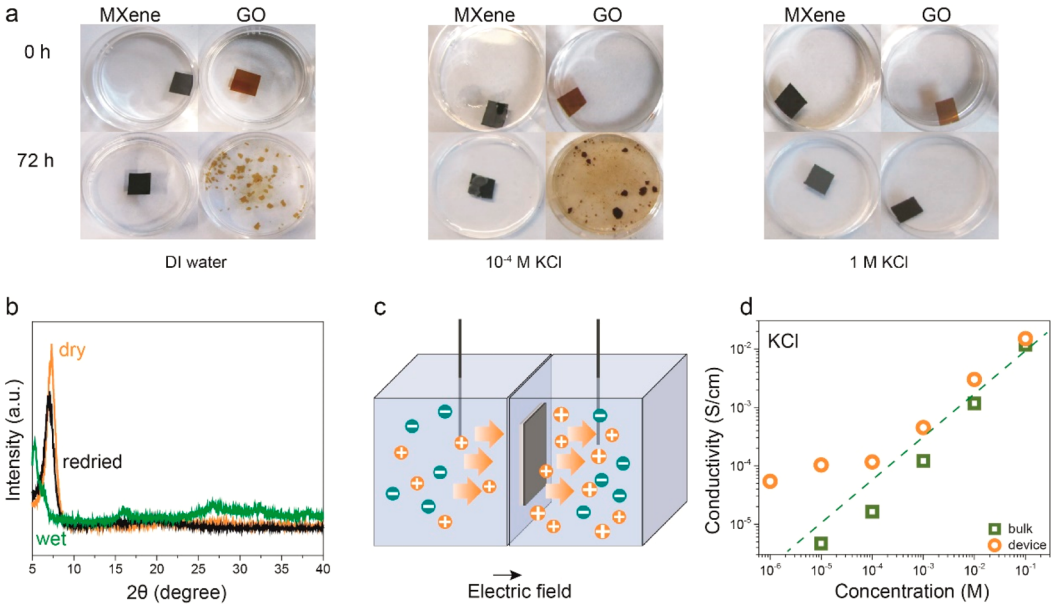

Figure 3. Structural stability in water. (a) Neat MXene membrane remained stable in DI water, 10^{-4} M KCl, and 1 M KCl solutions after 72 h of immersion. On the contrary, the neat GO membrane is only stable in high concentration (1 M) KCl solution. (b) XRD pattern of the MXene membrane before immersion (dry), after immersion (wet), and after redried, suggesting that its laminar structure is largely retained during these processes. (c) Schematic illustration showing that the aqueous stable MXene membrane (black) allows nanofluidic transport in the vertical configuration without PDMS matrix sealing. (d) Ionic conductivities for (c) measured in KCl solution, suggesting that the surface-charge-governed transport behavior is retained.

surface termination groups, especially the oxygen-containing groups. The charged MXene nanosheets electrostatically attract counterions (protons or cations here, as illustrated in Figure 2a), forming an electric double layer, whose thickness is characterized by the Debye length and is inversely proportional to the square root of electrolyte concentration.[45] At low concentrations, the Debye length is comparable to the nanochannel size. As a result, the ionic conductivity is dominated by the accumulated counterions whose amount is fixed by the MXene surface charge and is therefore largely independent of the ionic concentration. At high concentrations, however, the Debye length is negligible compared to the channel size, resulting in a bulk behavior. It is worth noting that this surface-charge-governed transport is maintained regardless of the electrolyte type, as shown in Figure 2e–g, where the ionic conductivities of KCl, NaCl, and $AlCl_3$ are presented (quantitative values are shown in Table S1), respectively. For all of these electrolytes, the ionic conductivities of the MXene membrane deviate from the bulk behavior at around 10^{-4} to 10^{-3} M, and the plateau conductivity at low concentrations is around 10^{-5} to 10^{-4} S/cm, independent of the membrane thickness (Figure S5). We also measured the pH values of all electrolytes (Table S2) and the ζ-potential of MXene at pH 1 to 14 (Figure S3). Results show that within the pH range of the various electrolytes, MXene has largely constant and negative ζ-potential, suggesting that the observed surface-charge-governed transport is not affected by the changing electrolyte pH. It is worth noting that for these electrolyte solutions, the proton concentration in water can be neglected (Table S2). These results are similar to those measured on a 2D BN nanofluidic membrane.[10]

A feature of 2D layered membranes for nanofluidics is their mechanical flexibility, which is favored for soft nanofluidic applications.[8] To demonstrate this, a piece of rectangular MXene membrane is bent, with its two ends embedded in PDMS and exposed to KCl electrolyte solution (Figure 2h). Figure 2i shows that the surface-governed transport behavior is well kept, and the conductivity is identical to that in Figure 2e.

From the surface-charge-governed ionic conductivity, it is possible to estimate the surface charge density of MXene nanosheets. The ionic conductance (G) is contributed by both the bulk electrolyte (denoted by G_{bulk}) and the surface charge (denoted by $G_{surface}$)[46]

$$G = G_{bulk} + G_{surface} = (\mu_{cation} + \mu_{anion})cN_A ewd/l + 2\mu_{cation}\sigma w/l \quad (1)$$

where μ_{cation} and μ_{anion} are the mobilities of the cation and anion, respectively, N_A Avogadro's number, c the bulk electrolyte concentration, e the elementary charge, w the width of the membrane, d the channel size, l the length of the membrane, and σ the surface charge density of MXene. From eq 1, we estimate σ to be around 0.06 mC/m^2 (see also Supplementary Note 1 in the Supporting Information). It is noteworthy that this value is about 1 order of magnitude smaller than that of the GO membrane, vermiculite membrane, and BN membrane. As a result, the ionic conductivity of the MXene membrane is also around 1–2 orders of magnitude lower than that of GO and the clay membrane[3,8] and slightly lower than that of the BN membrane.[10,47] Therefore, it is worth noting that the claimed fast transport of the MXene membrane here is compared to that of bulk rather than GO or clay membranes. However, the low surface charge density also enhances the membrane's structural stability in water, as demonstrated below.

Aqueous Stability. We demonstrate that one of the key advantages of the MXene membrane compared to GO or vermiculite clay membrane is its inherent high aqueous stability. It is known that neat GO or clay membranes are

DOI: 10.1021/acsnano.8b06708
ACS Nano 2018, 12, 12464–12471

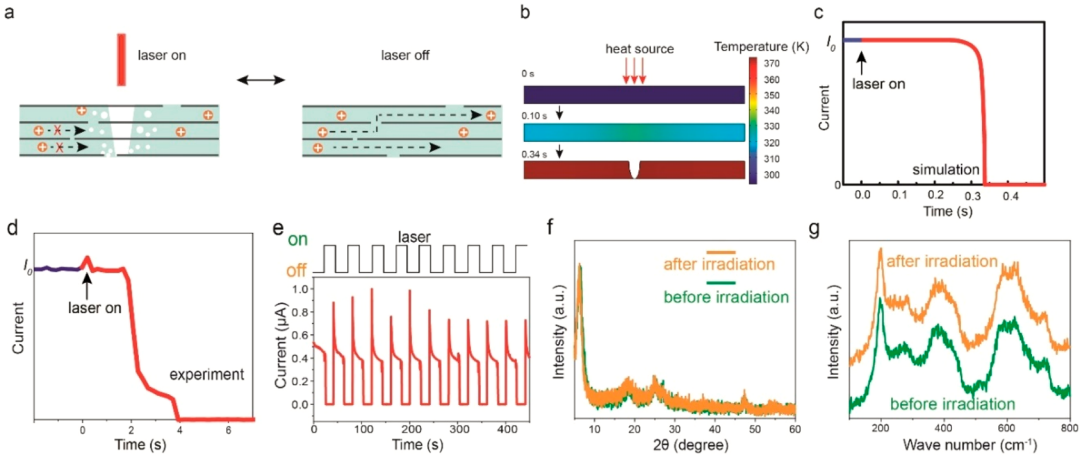

Figure 4. Photocontrolled transport through MXene membrane. (a) Schematic illustration of the photocontrolled transport mechanism. Upon laser irridation, the MXene rapidly heats up, vaporizing the interlayer water, and blocks the transport of ions. Note that the irradiated area is exposed to air to allow water to escape. When the laser is off, water rehydrates the membrane, allowing free transport of ions. (b) Numerical simulation of the temperature profile of the interlayer water (see details in the Supporting Information). Water in the irradiated region (marked with red arrows) is rapidly heated to boiling temperature and vaporized in about 0.34 s. (c) As a result, the ionic current rapidly decreaes from its initial value (I_0) to zero. (d) This is qualitatively in agreement with the experimental results. (e) Rapid and reversible switch of the ion transport. Similar XRD patterns (f) and Raman spectra (g) of the MXene membranes before and after laser irradiation, suggesting that the laser did not cause structural or chemical damage.

not stable in pure water or dilute monovalent electrolyte solutions, limiting their practical applications.[26] This is because lower concentration leads to the longer Debye length, therefore stronger intersheet electrostatic repulsive forces. Figure 3a shows that neat GO membrane stayed stable in 1 M KCl solution but disintegrated in 10^{-4} M KCl solution and DI water after 72 h of immersion, in line with a previous report.[26] Similar behavior was observed for the clay membrane (Figure S6). However, the neat MXene membrane remained stable in all conditions (Figure 3a), even after 1 month in DI water (Figure S7). In addition, its laminar structure is also well kept, as evidenced by the similar XRD patterns before and after immersion and drying (Figure 3b).

The stability of 2D membranes in water is mainly determined by the competition of van der Waals attractive force and electrostatic repulsive force between facing nanosheets. To understand the high aqueous stability of the MXene membrane, we first calculate its interlayer van der Waals interaction per unit area, $F_{\text{vdw-MXene}}$,[30] which is given by $F_{\text{vdw-MXene}} = H_{\text{MXene}}/6\pi d^3$, where H_{MXene} is the Hamaker's constant of the MXene membrane and d is the interlayer spacing. The Hamaker's constant can be derived with a textbook equation:[48]

$$H_{\text{MXene}} = \frac{3kT}{4}\left(\frac{\varepsilon - \varepsilon_{\text{water}}}{\varepsilon + \varepsilon_{\text{water}}}\right)^2 + \frac{3h\omega}{16\sqrt{2}}\frac{(n^2 - n_{\text{water}}^2)^2}{(n^2 + n_{\text{water}}^2)^{3/2}} \quad (2)$$

where k is the Boltzmann constant, T = 298 K the temperature, ε = 6.3 the dielectric constant of MXene,[49] n = 2.7 the refractive index of MXene,[49] $\varepsilon_{\text{water}}$ = 80 the dielectric constant of water, n_{water} = 1.33 the refractive index of water, h the Planck's constant, and $\omega = 4.73 \times 10^{14}$ s^{-1} the absorption frequency. As a result, H_{MXene} is calculated to be 4.87×10^{-20} J. In comparison, the Hamaker's constant of the GO membrane is around 5.47×10^{-21} J,[30] and that of vermiculite is around 5.50×10^{-21} J, considering that $n \approx 1.6$[50] and $\varepsilon \approx 3.0$[51] for vermiculite. Therefore, for a certain interlayer spacing, the interlayer van der Waals interaction of MXene is about 1 order of magnitude higher than that of GO or vermiculite, similar to that of the layered MoS_2 membrane.[30]

Furthermore, we analyze the interlayer electrostatic repulsive force. The electrostatic potential φ induced by the charged nanosheets in solution at distance d is given by $\varphi(d) = \varphi_s \exp(-d/\lambda)$, according to Debye–Huckel approximation,[45] with φ_s being the surface potential and λ being the Debye length. For small surface potential,[52] $\varphi_s \approx \sigma\lambda/\varepsilon\varepsilon_0$, where σ is the surface charge density. Therefore, the exerted electrostatic force on a facing nanosheet at distance d per unit area is estimated to be $F_{\text{elec}} = -\sigma\nabla\varphi \propto \sigma^2$. As the σ of MXene is about 1 order of magnitude smaller than that of GO or clay membrane, the electrostatic repulsive force is estimated to be around 2 orders of magnitude smaller. The dramatically decreased electrostatic repulsive force and increased van der Waals attraction force may semiquantitatively explain the high structural stability of the MXene membrane in water. A quantitative calculation might be feasible by coupling the electrostatic forces, van der Waals forces, and short-range chemical forces,[53] which is beyond the scope of this study.

The high aqueous stability of MXene is beneficial for its membrane applications without any further modifications. In previous studies, the nanofluidic transport properties of the neat 2D membrane are usually tested with a horizontal configuration (Figure 2b), such that the membrane can be embedded in the PDMS matrix to ensure the structural stability.[3,8,10] Most practical applications, however, require the vertical configuration to maximize the ionic flux.[9] Here, we demonstrate that the MXene membrane allows high flux nanofluidic transport in the vertical direction (schematic illustration in Figure 3c) without the help of cross-linkers. Representative ionic conductivities for KCl solution with different concentrations for a 5 μm thick membrane are shown in Figure 3d. Apparently, the ionic conductivity is similar to that with the horizontal configuration (Figure 2e), confirming that the nanofluidic transport property is independent of the configuration. This result suggests that if an ultrathin MXene

DOI: 10.1021/acsnano.8b06708
ACS Nano 2018, 12, 12464–12471

membrane is used, the ionic flux could be enhanced by orders of magnitude, allowing ultrafast mass transport. It is worthwhile to note that, in the vertical configuration, the edge surface charge of the MXene nanosheets may also affect the ion transport. The similar ionic transport behaviors of vertical and horizontal configurations suggest that the edge chemical state may also contribute to the ionic conductivity in the horizontal configuration, on top of the in-plane surface charge of MXene nanosheets. Such effect is of interest to explore in future studies.

Photocontrolled Transport. A particular advantage of 2D materials for nanofluidics is their broad range of intrinsic and mechanical, electrical, optical, and chemical properties.[54,55] These properties could allow the manipulation of nanofluidic transport in an easy way. Of great interest is the remote manipulation with light, which enables on-demand switching of the membrane transport properties without direct contact. Here, by a simple proof-of-concept experiment, we demonstrate that the transport through the MXene membrane can be completely switched on and off with laser light within a few seconds. The mechanism is straightforward due to the superior photothermal effect of MXene.[56,57] It has been demonstrated that MXene can convert light to heat with nearly 100% efficiency.[56] As illustrated in Figure 4a, without laser irradiation, ions can transport through the membrane freely. Upon laser irradiation, the MXene membrane will rapidly heat up, which should vaporize the water in the layer spacing. Therefore, the water transport and ionic transport through the membrane will be completely shut off. To demonstrate this, a 2 μm thick MXene membrane was irradiated with a laser with a wavelength of 808 nm and a fixed power density of 2 W/m^2. Note that the irradiated area was not covered with PDMS (Figure 4a), to allow vaporized water to escape. Strong photothermal property was observed for our membrane, which could even burn the polymers underneath the membrane (Figure S9).

To support the photothermal vaporization mechanism, we performed numerical simulations. A 2 μm thick (corresponding to 0.8 μm thick interlayer water) and 20000 μm long MXene membrane was irradiated with laser of power 2 W/cm^2 (see details in the Supporting Information). The water temperature quickly increases when the laser is on (Figure 4b; color profile represents temperature of water; height and length were not drawn to scale for clarity), and after 0.3 s, water reaches a boiling temperature. Further laser irradiation causes the water inside the laser spot to vaporize (middle blank hole in the bottom scheme). Resultantly, the ionic current quickly drops to zero in 0.34 s (Figure 4c). To verify this simulation, we measured the weight loss of the membrane under prelonged laser irradiation (Figure S10), and the derived vaporization rate is indeed close to our simulation. It should be noted that when the membrane is dry or the membrane is completely sealed with PDMS, no weight loss was observed, further confirming the vaporization mechanism (Figure S10). In addition, the change of ionic current upon laser irradiation is also qualitatively in agreement with the simulation (Figure 4d). Quantitatively, the switching speed is slower than expected, possibly caused by the local chaotic water flow during vaporization which distorts ionic transport.

More importantly, such a switch is highly reversible, as shown by the fast and continuous switching in Figure 4e. The reversible switching can also be realized on much thicker MXene membranes (Figure S11). Moreover, the membrane was characterized with XRD (Figure 4f) and Raman (Figure 4g) before and after laser irradiation. No obvious changes were observed, suggesting that the laser did not cause structural or chemical damages to the membrane.[58] In previous studies, photocontrolled nanofluidic transport extensively relied on photosensitive molecules. Such photochemical approaches are generally inefficient and showed low on/off ratio. The physical method *via* photothermal effect induced cavitation is much more straightforward and crisper.

CONCLUSIONS

In summary, we demonstrate that the Ti_3C_2 membrane serves as an excellent nanofluidic platform. First, the ionic transport is surface-charge-governed, and the ionic conductivity can be 1−2 orders of magnitude higher than that in bulk. Enhancing the surface charge density and optimizing the interlayer spacing in future studies should lead to even larger conductivity. Second and more importantly, the membrane is highly stable in an aqueous environment, which enables high flux cross-membrane ion transport without any cross-linkers. This may inspire more exploration on aqueous stable 2D nanofluidic platforms, for which MoS_2 and other MXene membranes are excellent candidates.[29] Third, we demonstrate that transport through the Ti_3C_2 membrane can be easily controlled with light by making use of its superior photothermal effect. These results contribute to the understanding of ionic transport in the MXene membrane, which is beneficial for its broad nanofluidic applications. Furthermore, we expect the light-controlled transport to find applications as a smart separation membrane. This study suggests the possibilities to design 2D nanofluidic membranes by exploiting their electrical, optical, and/or chemical properties.

METHODS

Fabrication and Characterization of Materials. Ti_3AlC_2 powder (200 mesh, Materials Research Centre, Ukraine) was immersed in concentrated HF at room temperature and stirred for 12 h. Then it was dried in a vacuum oven for 24 h at 80 °C and blended with dimethyl sulfoxide (DMSO, Aladdin, China) and stirred at 310 K for 24 h to allow intercalation. After intercalation, excess DMSO was removed by washing with DI water and centrifugation at 4000 rpm several times. Finally, the solution was sonicated, and the few-layer MXene nanosheet was obtained. The MXene membrane was fabricated by vacuum filtration of the colloidal solution of MXene nanosheets with a Celgard 2400 membrane to avoid unintentional cross-linking. The thickness of the MXene nanosheet was characterized with atomic force microscopy (NTEGRA Spectra). The thickness of the membrane was typically a few micrometers, determined by a cross-sectional SEM image (HITACHI S-4800). X-ray diffraction patterns were carried out on DX-27 mini with Cu Kα radiation. X-ray photoelectron spectroscopy (XPS) was performed on Physical Electronics PHI5802 instrument using a magnesium anode (monochromatic Kα X-rays at 253.6 eV) as the source. The binding energy in the XPS spectra was calibrated with a carbon signal (C 1s at 284.6 eV). Neat GO and vermiculite clay nanosheets were fabricated according to previous reports[3,26] and assembled into the membrane with the same vacuum filtration method on polymeric filter.

Preparation and Characterization of the Nanofluidic Devices. The MXene membrane was sliced into a rectangular shape. The membrane length is at the centimeter scale and width is at the millimeter scale. The exact size for each sample is measured to calculate conductivity. In our experiment, the conductivity is not dependent on the size. Then the sample was immersed into the PDMS precursor, which was cured in oven for 5 h at 80 °C. After that, two reservoirs were carved out at the ends of the MXene strip. The two ends of the strip were exposed to the various electrolyte

DOI: 10.1021/acsnano.8b06708
ACS Nano 2018, 12, 12464−12471

concentrations of 10^{-6}–10^{0} M. Two Ag/AgCl electrodes were inserted into the reservoirs to measure the current with a bias voltage applied. The I–V curve was recorded with a Keithley 2400 instrument. The ionic conductivities were calculated based on the I–V curves, dimensions of the membrane, and interlayer spacing following previous work.[8]

ASSOCIATED CONTENT

Supporting Information

The Supporting Information is available free of charge on the ACS Publications website at DOI: 10.1021/acsnano.8b06708.

Characterization of MXene, structure stability, photothermal effect, and thickness-dependent ionic current of MXene (PDF)

AUTHOR INFORMATION

Corresponding Authors

*E-mail: jun.gao@utwente.nl.

*E-mail: jluo@tju.edu.cn.

ORCID

Jinsong Wu: 0000-0002-7305-7927

Jiayan Luo: 0000-0002-4619-6040

Notes

The authors declare no competing financial interest.

ACKNOWLEDGMENTS

The authors appreciate support from National Natural Science Foundation of China (Grant Nos. 51872196, U1601206, and 51502197), Natural Science Foundation of Tianjin, China (Grant Nos. 17JCJQJC44100 and 15JCYBJC53100), and the 111 Project of B12015.

REFERENCES

(1) Dikin, D. A.; Stankovich, S.; Zimney, E. J.; Piner, R. D.; Dommett, G. H.; Evmenenko, G.; Nguyen, S. T.; Ruoff, R. S. Preparation and Characterization of Graphene Oxide Paper. *Nature* **2007**, *448*, 457–460.

(2) Gao, J.; Feng, Y.; Guo, W.; Jiang, L. Nanofluidics in Two-Dimensional Layered Materials: Inspirations from Nature. *Chem. Soc. Rev.* **2017**, *46*, 5400–5424.

(3) Shao, J.-J.; Raidongia, K.; Koltonow, A. R.; Huang, J. Self-Assembled Two-Dimensional Nanofluidic Proton Channels with High Thermal Stability. *Nat. Commun.* **2015**, *6*, 7602.

(4) Cheng, C.; Jiang, G.; Garvey, C. J.; Wang, Y.; Simon, G. P.; Liu, J. Z.; Li, D. Ion Transport in Complex Layered Graphene-Based Membranes with Tuneable Interlayer Spacing. *Sci. Adv.* **2016**, *2*, e1501272.

(5) Yang, X. W.; Cheng, C.; Wang, Y. F.; Qiu, L.; Li, D. Liquid-Mediated Dense Integration of Graphene Materials for Compact Capacitive Energy Storage. *Science* **2013**, *341*, 534–537.

(6) Joshi, R. K.; Carbone, P.; Wang, F. C.; Kravets, V. G.; Su, Y.; Grigorieva, I. V.; Wu, H. A.; Geim, A. K.; Nair, R. R. Precise and Ultrafast Molecular Sieving Through Graphene Oxide Membranes. *Science* **2014**, *343*, 752–754.

(7) Abraham, J.; Vasu, K. S.; Williams, C. D.; Gopinadhan, K.; Su, Y.; Cherian, C. T.; Dix, J.; Prestat, E.; Haigh, S. J.; Grigorieva, I. V.; Carbone, P.; Geim, A. K.; Nair, R. R. Tunable Sieving of Ions Using Graphene Oxide Membranes. *Nat. Nanotechnol.* **2017**, *12*, 546–551.

(8) Raidongia, K.; Huang, J. Nanofluidic Ion Transport through Reconstructed Layered Materials. *J. Am. Chem. Soc.* **2012**, *134*, 16528–16531.

(9) Koltonow, A. R.; Huang, J. Two-dimensional Nanofluidics. *Science* **2016**, *351*, 1395–1396.

(10) Qin, S.; Liu, D.; Wang, G.; Portehault, D.; Garvey, C. J.; Gogotsi, Y.; Lei, W.; Chen, Y. High and Stable Ionic Conductivity in 2D Nanofluidic Ion Channels between Boron Nitride Layers. *J. Am. Chem. Soc.* **2017**, *139*, 6314–6320.

(11) Stein, D.; Kruithof, M.; Dekker, C. Surface-Charge-Governed Ion Transport in Nanofluidic Channels. *Phys. Rev. Lett.* **2004**, *93*, 035901.

(12) Xiao, K.; Giusto, P.; Wen, L.; Jiang, L.; Antonietti, M. Nanofluidic Ion Transport and Energy Conversion through Ultrathin Free-Standing Polymeric Carbon Nitride Membranes. *Angew. Chem.* **2018**, *130*, 10280–10283.

(13) Liu, G.; Jin, W.; Xu, N. Two-Dimensional-Material Membranes: A New Family of High-Performance Separation Membranes. *Angew. Chem., Int. Ed.* **2016**, *55*, 13384–13397.

(14) Sun, P.; Wang, K.; Zhu, H. Recent Developments in Graphene-Based Membranes: Structure, Mass-Transport Mechanism and Potential Applications. *Adv. Mater.* **2016**, *28*, 2287–2310.

(15) Hu, M.; Mi, B. Enabling Graphene Oxide Nanosheets as Water Separation Membranes. *Environ. Sci. Technol.* **2013**, *47*, 3715–3723.

(16) Han, Y.; Xu, Z.; Gao, C. Ultrathin Graphene Nanofiltration Membrane for Water Purification. *Adv. Funct. Mater.* **2013**, *23*, 3693–3700.

(17) Sun, P.; Zheng, F.; Zhu, M.; Wang, K.; Zhong, M.; Wu, D.; Zhu, H. Realizing Synchronous Energy Harvesting and Ion Separation with Graphene Oxide Membranes. *Sci. Rep.* **2015**, *4*, 5528.

(18) Ji, J.; Kang, Q.; Zhou, Y.; Feng, Y.; Chen, X.; Yuan, J.; Guo, W.; Wei, Y.; Jiang, L. Osmotic Power Generation with Positively and Negatively Charged 2D Nanofluidic Membrane Pairs. *Adv. Funct. Mater.* **2017**, *27*, 1603623.

(19) Gao, W.; Singh, N.; Song, L.; Liu, Z.; Reddy, A. L. M.; Ci, L.; Vajtai, R.; Zhang, Q.; Wei, B.; Ajayan, P. M. Direct Laser Writing of Micro-Supercapacitors on Hydrated Graphite Oxide Films. *Nat. Nanotechnol.* **2011**, *6*, 496–500.

(20) Liu, S.; Tang, S.; Zhang, X.; Wang, A.; Yang, Q. H.; Luo, J. Porous Al Current Collector for Dendrite-Free Na Metal Anodes. *Nano Lett.* **2017**, *17*, 5862–5868.

(21) Liu, S.; Wang, A.; Li, Q.; Wu, J.; Chiou, K.; Huang, J.; Luo, J. Crumpled Graphene Balls Stabilized Dendrite-Free Lithium Metal Anodes. *Joule* **2018**, *2*, 184–193.

(22) Wang, A.; Hu, X.; Tang, H.; Zhang, C.; Liu, S.; Yang, Y.; Yang, Q.; Luo, J. Processable and Moldable Sodium Metal Anodes. *Angew. Chem., Int. Ed.* **2017**, *56*, 11921–11926.

(23) Wang, A.; Tang, S.; Kong, D.; Liu, S.; Chiou, K.; Zhi, L.; Huang, J.; Xia, Y. Y.; Luo, J. Bending-Tolerant Anodes for Lithium-Metal Batteries. *Adv. Mater.* **2018**, *30*, 1703891.

(24) Huang, J.; Zhuang, T.; Zhang, Q.; Peng, H.; Chen, C.; Wei, F. Permselective Graphene Oxide Membrane for Highly Stable and Anti-Self-Discharge Lithium–Sulfur Batteries. *ACS Nano* **2015**, *9*, 3002–3011.

(25) Gao, W.; Wu, G.; Janicke, M. T.; Cullen, D. A.; Mukundan, R.; Baldwin, J. K.; Brosha, E. L.; Galande, C.; Ajayan, P. M.; More, K. L.; Dattelbaum, A. M.; Zelenay, P. Ozonated Graphene Oxide Film as a Proton-Exchange Membrane. *Angew. Chem., Int. Ed.* **2014**, *53*, 3588–3593.

(26) Yeh, C.-N.; Raidongia, K.; Shao, J.; Yang, Q.-H.; Huang, J. On the Origin of the Stability of Graphene Oxide Membranes in Water. *Nat. Chem.* **2015**, *7*, 166–170.

(27) Carroll, D. *Ion Exchange in Clays and Other Minerals*; Geological Society of America Bulletin, 1959; pp 749–779.

(28) Pei, S.; Cheng, H.-M. The Reduction of Graphene Oxide. *Carbon* **2012**, *50*, 3210–3228.

(29) Deng, M.; Kwac, K.; Li, M.; Jung, Y.; Park, H. G. Stability, Molecular Sieving, and Ion Diffusion Selectivity of a Lamellar Membrane from Two-Dimensional Molybdenum Disulfide. *Nano Lett.* **2017**, *17*, 2342–2348.

(30) Wang, Z.; Tu, Q.; Zheng, S.; Urban, J. J.; Li, S.; Mi, B. Understanding the Aqueous Stability and Filtration Capability of MoS_2 Membranes. *Nano Lett.* **2017**, *17*, 7289–7298.

(31) Hou, X.; Guo, W.; Jiang, L. Biomimetic Smart Nanopores and Nanochannels. *Chem. Soc. Rev.* **2011**, *40*, 2385–2401.

DOI: 10.1021/acsnano.8b06708
ACS Nano 2018, 12, 12464–12471

(32) Liu, J.; Wang, N.; Yu, L. J.; Karton, A.; Li, W.; Zhang, W.; Guo, F.; Hou, L.; Cheng, Q.; Jiang, L.; Weitz, D. A.; Zhao, Y. Bioinspired Graphene Membrane with Temperature Tunable Channels for Water Gating and Molecular Separation. *Nat. Commun.* **2017**, *8*, 2011.
(33) Zhou, K. G.; Vasu, K. S.; Cherian, C. T.; Neek-Amal, M.; Zhang, J. C.; Ghorbanfekr-Kalashami, H.; Huang, K.; Marshall, O. P.; Kravets, V. G.; Abraham, J.; Su, Y.; Grigorenko, A. N.; Pratt, A.; Geim, A. K.; Peeters, F. M.; Novoselov, K. S.; Nair, R. R. Electrically Controlled Water Permeation Through Graphene Oxide Membranes. *Nature* **2018**, *559*, 236−240.
(34) Cheng, C.; Jiang, G.; Simon, G. P.; Liu, J. Z.; Li, D. Low-Voltage Electrostatic Modulation of Ion Diffusion Through Layered Graphene-Based Nanoporous Membranes. *Nat. Nanotechnol.* **2018**, *13*, 685−690.
(35) Naguib, M.; Kurtoglu, M.; Presser, V.; Lu, J.; Niu, J.; Heon, M.; Hultman, L.; Gogotsi, Y.; Barsoum, M. W. Two-Dimensional Nanocrystals Produced by Exfoliation of Ti_3AlC_2. *Adv. Mater.* **2011**, *23*, 4248−4253.
(36) Augustyn, V.; Gogotsi, Y. 2D Materials with Nanoconfined Fluids for Electrochemical Energy Storage. *Joule* **2017**, *1*, 443−452.
(37) Ghidiu, M.; Lukatskaya, M. R.; Zhao, M.-Q.; Gogotsi, Y.; Barsoum, M. W. Conductive Two-Dimensional Titanium Carbide 'Clay' with High Volumetric Capacitance. *Nature* **2014**, *516*, 78−81.
(38) Lukatskaya, M. R.; Mashtalir, O.; Ren, C. E.; Dall'Agnese, Y.; Rozier, P.; Taberna, P. L.; Naguib, M.; Simon, P.; Barsoum, M. W.; Gogotsi, Y. Cation Intercalation and High Volumetric Capacitance of Two-Dimensional Titanium Carbide. *Science* **2013**, *341*, 1502−1505.
(39) Zhang, C.; Kremer, M. P.; Seral-Ascaso, A.; Park, S.-H.; McEvoy, N.; Anasori, B.; Gogotsi, Y.; Nicolosi, V. Stamping of Flexible, Coplanar Micro-Supercapacitors Using MXene Inks. *Adv. Funct. Mater.* **2018**, *28*, 1705506.
(40) Ding, L.; Wei, Y.; Wang, Y.; Chen, H.; Caro, J.; Wang, H. A Two-Dimensional Lamellar Membrane: MXene Nanosheet Stacks. *Angew. Chem., Int. Ed.* **2017**, *56*, 1825−1829.
(41) Peng, Q.; Guo, J.; Zhang, Q.; Xiang, J.; Liu, B.; Zhou, A.; Liu, R.; Tian, Y. Unique Lead Adsorption Behavior of Activated Hydroxyl Group in Two-Dimensional Titanium Carbide. *J. Am. Chem. Soc.* **2014**, *136*, 4113−4116.
(42) Liu, J.; Zhang, H. B.; Sun, R.; Liu, Y.; Liu, Z.; Zhou, A.; Yu, Z. Z. Hydrophobic, Flexible, and Lightweight MXene Foams for High Performance Electromagnetic-Interference Shielding. *Adv. Mater.* **2017**, *29*, 1702367.
(43) Mashtalir, O.; Naguib, M.; Mochalin, V. N.; Dall'Agnese, Y.; Heon, M.; Barsoum, M. W.; Gogotsi, Y. Intercalation and Delamination of Layered Carbides and Carbonitrides. *Nat. Commun.* **2013**, *4*, 1716.
(44) Ding, L.; Wei, Y.; Li, L.; Zhang, T.; Wang, H.; Xue, J.; Ding, L. X.; Wang, S.; Caro, J.; Gogotsi, Y. MXene Molecular Sieving Membranes for Highly Efficient Gas Separation. *Nat. Commun.* **2018**, *9*, 155.
(45) Schoch, R. B.; Han, J.; Renaud, P. Transport Phenomena in Nanofluidics. *Rev. Mod. Phys.* **2008**, *80*, 839−883.
(46) Schoch, R. B.; Renaud, P. Ion Transport through Nanoslits Dominated by the Effective Surface Charge. *Appl. Phys. Lett.* **2005**, *86*, 253111−253113.
(47) Qin, S.; Liu, D.; Chen, Y.; Chen, C.; Wang, G.; Wang, J.; Razal, J. M.; Lei, W. Nanofluidic Electric Generators Constructed from Boron Nitride Nanosheets Membranes. *Nano Energy* **2018**, *47*, 368−373.
(48) Israelachvili, J. N. *Intermolecular and surface forces*; Academic Press, 2011; pp 107−132.
(49) Satheeshkumar, E.; Makaryan, T.; Melikyan, A.; Minassian, H.; Gogotsi, Y.; Yoshimura, M. One-Step Solution Processing of Ag, Au and Pd@MXene Hybrids for SERS. *Sci. Rep.* **2016**, *6*, 32049.
(50) Coleman, N.; LeRoux, F.; Cady, J. G. Biotite - Hydrobiotite - Vermiculite in Soils. *Nature* **1963**, *198*, 409.
(51) Anjos, I. F. D.; Fontgalland, G.; Freire, R. S. C.; Barbin, S. E.; Lira, B. B. Vermiculite dielectric constant measurement using a volumetric water content probe. *IEEE International Instrumentation and Measurement Technology Conference (I2MTC)* **2011**, 1−5.
(52) Butt, H.; Graf, K.; Kappl, M. *Physics and Chemistry of Interfaces*; Wiley-VCH Verlag GmbH & Co. KGaA, 2004; pp 42−56.
(53) Mugele, F.; Bera, B.; Cavalli, A.; Siretanu, I.; Maestro, A.; Duits, M.; Cohen-Stuart, M.; van den Ende, D.; Stocker, I.; Collins, I. Ion Adsorption-Induced Wetting Transition in Oil-Water-Mineral Systems. *Sci. Rep.* **2015**, *5*, 10519.
(54) Novoselov, K. S.; Fal'ko, V. I.; Colombo, L.; Gellert, P. R.; Schwab, M. G.; Kim, K. A. Roadmap for Graphene. *Nature* **2012**, *490*, 192−200.
(55) Butler, S. Z.; Hollen, S. M.; Cao, L.; Cui, Y.; Gupta, J. A.; Gutiérrez, H. R.; Heinz, T. F.; Hong, S. S.; Huang, J.; Ismach, A. F.; Johnston-Halperin, E.; Kuno, M.; Plashnitsa, V. V.; Robinson, R. D.; Ruoff, R. S.; Salahuddin, S.; Shan, J.; Shi, L.; Spencer, M. G.; Terrones, M.; et al. Progress, Challenges, and Opportunities in Two-Dimensional Materials beyond Graphene. *ACS Nano* **2013**, *7*, 2898−2926.
(56) Li, R.; Zhang, L.; Shi, L.; Wang, L. P. MXene Ti_3C_2: An Effective 2D Light-to-Heat Conversion Material. *ACS Nano* **2017**, *11*, 3752−3759.
(57) Lin, H.; Wang, X.; Yu, L.; Chen, Y.; Shi, J. Two-Dimensional Ultrathin MXene Ceramic Nanosheets for Photothermal Conversion. *Nano Lett.* **2017**, *17*, 384−391.
(58) Zhang, C. J.; Pinilla, S.; McEvoy, N.; Cullen, C. P.; Anasori, B.; Long, E.; Park, S.-H.; Seral-Ascaso, A.; Shmeliov, A.; Krishnan, D.; Morant, C.; Liu, X.; Duesberg, G. S.; Gogotsi, Y.; Nicolosi, V. Oxidation Stability of Colloidal Two-Dimensional Titanium Carbides (MXenes). *Chem. Mater.* **2017**, *29*, 4848−4856.

DOI: 10.1021/acsnano.8b06708
ACS Nano 2018, 12, 12464−12471